Extreme Storm Surge Events and Associated Dynamics in the North Atlantic

Simon Barbot, Lucia Pineau-Guillou, Jean Marc Delouis

JGR Oceans

RESEARCH ARTICLE
10.1029/2023JC020772

Extreme Storm Surge Events and Associated Dynamics in the North Atlantic

Simon Barbot[1], **Lucia Pineau-Guillou**[1], and **Jean-Marc Delouis**[1]

[1]Laboratoire d'Océanographie Physique et Spatiale, UMR 6523 (IFREMER, CNRS, IRD, UBO), IUEM, Brest, France

Abstract Storm surges events are investigated using the ECHAR method, which identifies and quantifies the different dynamical structures of a typical storm surge event. In the North Atlantic, analysis of 65 tide gauges revealed that storm surge events display two major and two minor structures, each of them corresponding to specific ocean dynamics. The two major structures refer to a slow-time Gaussian structure, lasting around 24 days, associated with the impact of the atmospheric pressure and a fast-time Laplace structure, lasting around 1.4 days, mainly wind-driven. The absence of the Gaussian structure along the North America coasts is explained by storms of smaller spatial extension, compared to Europe. Concerning the minor structures, a negative surge of around 6 cm just after the peak surge is observed over North America only. Such a sudden drop of the sea level is explained by the turning winds during the storm event, favored by the smaller spatial extension of storms. Finally, high frequency oscillations, with amplitude typically of 3 cm and up to 25 cm, are observed at some tide gauges. These oscillations refer to tide-surge interactions and they are often maximum at a specific phase of the tide and/or enhanced because of resonant basins.

Plain Language Summary The storm surges refer to the extreme values of the sea level time series, after the removal of tides and the mean sea level. The storm surges are due to extreme weather systems such as storms and are responsible for coastal flooding. Rather than focusing on the maximum values of the sea level during storm events, we consider the full dynamics of the events from 20 days before to 20 days after each maximum. Doing so helps to properly describe the different types of storm surge events and explain the atmospheric and ocean dynamics leading to such extremes.

Key Points:

- The new ECHAR method decomposes storm surge events in two major and two minor structures each of them reflecting specific ocean dynamics
- In North America a large drop of the sea level 1.5 days after the peak surge is explained by turning winds and storms of small extent
- Observed oscillations with amplitude up to 10 cm are the signature of tide-surge interaction

Supporting Information:

Supporting Information may be found in the online version of this article.

Correspondence to:

S. Barbot,
simon.barbot@ifremer.fr

Citation:

Barbot, S., Pineau-Guillou, L., & Delouis, J.-M. (2024). Extreme storm surge events and associated dynamics in the North Atlantic. *Journal of Geophysical Research: Oceans*, *129*, e2023JC020772. https://doi.org/10.1029/2023JC020772

Received 15 DEC 2023
Accepted 3 JUL 2024

Author Contributions:

Conceptualization: Simon Barbot, Lucia Pineau-Guillou
Data curation: Simon Barbot, Lucia Pineau-Guillou
Formal analysis: Simon Barbot
Funding acquisition: Lucia Pineau-Guillou
Investigation: Simon Barbot
Methodology: Simon Barbot, Lucia Pineau-Guillou, Jean-Marc Delouis
Project administration: Lucia Pineau-Guillou
Resources: Simon Barbot
Software: Simon Barbot, Lucia Pineau-Guillou
Supervision: Lucia Pineau-Guillou, Jean-Marc Delouis

1. Introduction

The surge refers to the sea level elevation after removing the Mean Sea Level (MSL) and the predicted tides. Surges are mainly due to atmospheric pressure gradient and the wind stress (Gill, 1982; Pugh & Woodworth, 2014). Other processes, such as wave breaking (e.g., Lavaud et al., 2020), tsunami, meteo-tsunami and seiches can also contribute to the surge, but generally, to a smaller proportion in the North Atlantic. Extreme surges mainly occur during storms: the strong decrease of atmospheric pressure and the associated strong winds provoke storm surges that can be several meters high, causing human loss and damages due to the floods of the coastal areas (e.g., Haigh et al., 2022; Hague et al., 2022). In the future, extreme sea level events are expected to become more and more frequent, due to sea level rise (Seneviratne et al., 2021). Extreme sea level events occurring now every century, will occur annually or more frequently by 2050 at 19%–31% of the tide gauges (Oppenheimer et al., 2019; Seneviratne et al., 2021). It is then essential to investigate all aspects of storm surges, in order to anticipate future changes.

In the North Atlantic, weather extremes may be due to tropical or extratropical storms (Booth et al., 2021; Catalano & Broccoli, 2018; Davis & Dolan, 1993; Feser et al., 2015; Hoskins & Hodges, 2002; Priestley et al., 2020). Even if their tracks may be similar along the North American coasts, their physics are completely different. Tropical storms need a sea surface temperature above 27°C to be formed. In these warm conditions, specific successive convection cells can build up and create a very low pressure at its center, and high wind speed in surrounding areas. Differently, extratropical storms are enhanced by the orography above the Rocky Mountains and the land-sea contrast (Brayshaw et al., 2009), which provokes strong wind fields across large-scale atmospheric fronts. In the present study, we focus on extratropical storms only, which occur during the winter period.

Most of the studies about storm surges focus on the peak surge (i.e., the maximum elevation of the surges during a stormy event) and investigate its statistics (e.g., mean intensity, return periods, timing, frequency of

Validation: Simon Barbot, Lucia Pineau-Guillou, Jean-Marc Delouis
Visualization: Simon Barbot
Writing – original draft: Simon Barbot
Writing – review & editing: Simon Barbot, Lucia Pineau-Guillou, Jean-Marc Delouis

occurrence; Baranes et al., 2020; Haigh et al., 2016; Jenkins et al., 2023; Marcos & Woodworth, 2017; Munroe & Curtis, 2017), how they evolve over time (Enríquez et al., 2022; Reinert et al., 2021; Talke et al., 2014; Wahl & Chambers, 2015) and what are their trends (Falasca et al., 2023; Marcos & Woodworth, 2017; Menéndez & Woodworth, 2010). In addition to the peak surge, some studies also focus on the duration of the storm surge events, defined as the elapsed time over a given threshold (Cid et al., 2016; Haigh et al., 2010; Zhang et al., 2000).

Beyond the peak surge, the full dynamics of the storm surge event (storm surge hourly time series) over a few days is rarely investigated statistically. Generally, only a few individual storms in specific areas are investigated because they are the strongest or associated with the highest damages. For example, three storms in Northern Europe in Wolf and Flather (2005), four storms in the North Sea in Pineau-Guillou et al. (2020), three storms along the Danish coastlines in Andrée et al. (2021). Only few studies attempted to model statistically the full dynamics of the storm surge events, using a stochastic storm surge model they can generate many artificial events for the North Sea (Wahl et al., 2011) and the Baltic Sea (MacPherson et al., 2019). More recently, Pineau-Guillou et al. (2023) proposed the ECHAR method (Event CHARacterization), to characterize statistically the full dynamics of typical storm surge events. Applying this method in the North-East Atlantic tide gauges, revealed that storm surge events displayed in this region a slow-time structure (mostly pressure driven) and a fast-time structure (mostly wind driven), lasting about 16 and 1.7 days respectively.

The present study aims to investigate the temporal dynamics of the storm surge events in the North Atlantic, using an improved version of the ECHAR method. We focus on the geographic diversity of the storm surge events rather than the diversity in one place. The study is organized as follows: Section 2 describes the sea level and atmospheric data, Section 3 details the improved ECHAR method, Section 4 presents the main patterns of the typical storm surge events. Finally, Section 5 summarizes and discusses the results.

2. Data

2.1. Sea Level Data

The hourly sea level measurements are extracted from GESLA 3.0 tide gauge data set (Caldwell & Merrifield, 2015; Haigh et al., 2022; Woodworth et al., 2016), when the time series are longer than 80 years. In the North Atlantic (longitude from 100°E to 20°E, latitude from 10°N to 20°N), 65 tide gauges are selected: 29 along the North American coasts and 36 along the European coasts (Figure 1a). Note that 17 tide gauges were considered despite having only between 50 and 80 years of data (light blue in Figure 1b), to fill the spatial gaps and enrich the analysis. The years with less than only 75% of hourly data are discarded (Baranes et al., 2020; Menéndez & Woodworth, 2010; Wahl & Chambers, 2015, white gaps in the timelines, Figure 1b).

Surges are computed by removing the predicted tides and the MSL from the hourly sea level data. The predicted tides are computed from the harmonic analysis of 75 tidal constituents for each year with a 20-year sliding window using the Tidal Toolbox (Allain, 2014). This allows to take into account any change in the tide (Haigh et al., 2020; Pineau-Guillou et al., 2021). The MSL is computed for each year from the detided sea level. Note that removing the yearly MSL allows to remove any trend related to MSL rise.

This study focuses on storm surges from extratropical storms. In order to exclude the tropical ones (i.e., tropical cyclones), storm surge events are only selected over winter, defined here from October to March, which is close to previous studies (e.g., October to March in Marcos & Woodworth, 2017 and in Pineau-Guillou et al., 2023). Note that other studies define the winter as a shorter period, generally from December to February for studies about the winter storminess and storm tracks (Feser et al., 2015; Gan & Wu, 2014; Hoskins & Hodges, 2019; Marciano et al., 2015), or from November to April for some studies about winter storm surges (Baranes et al., 2020; Thompson et al., 2013; Wahl & Chambers, 2015). Even if the North American storms that occur in October and November can be both from tropical and extratropical cyclones (Booth et al., 2021; Davis & Dolan, 1993; Zhang et al., 2000), removing those two months would exclude major extratropical storms along the European coasts (e.g., the 1987 Great Storm; Burt & Mansfield, 1988). For this reason, we considered the winter from October 1st to March 31st. Note that the root mean square error (RMSE) between the typical event with or without October and November has an average of 1 cm, so this choice has no impact on the results of this study.

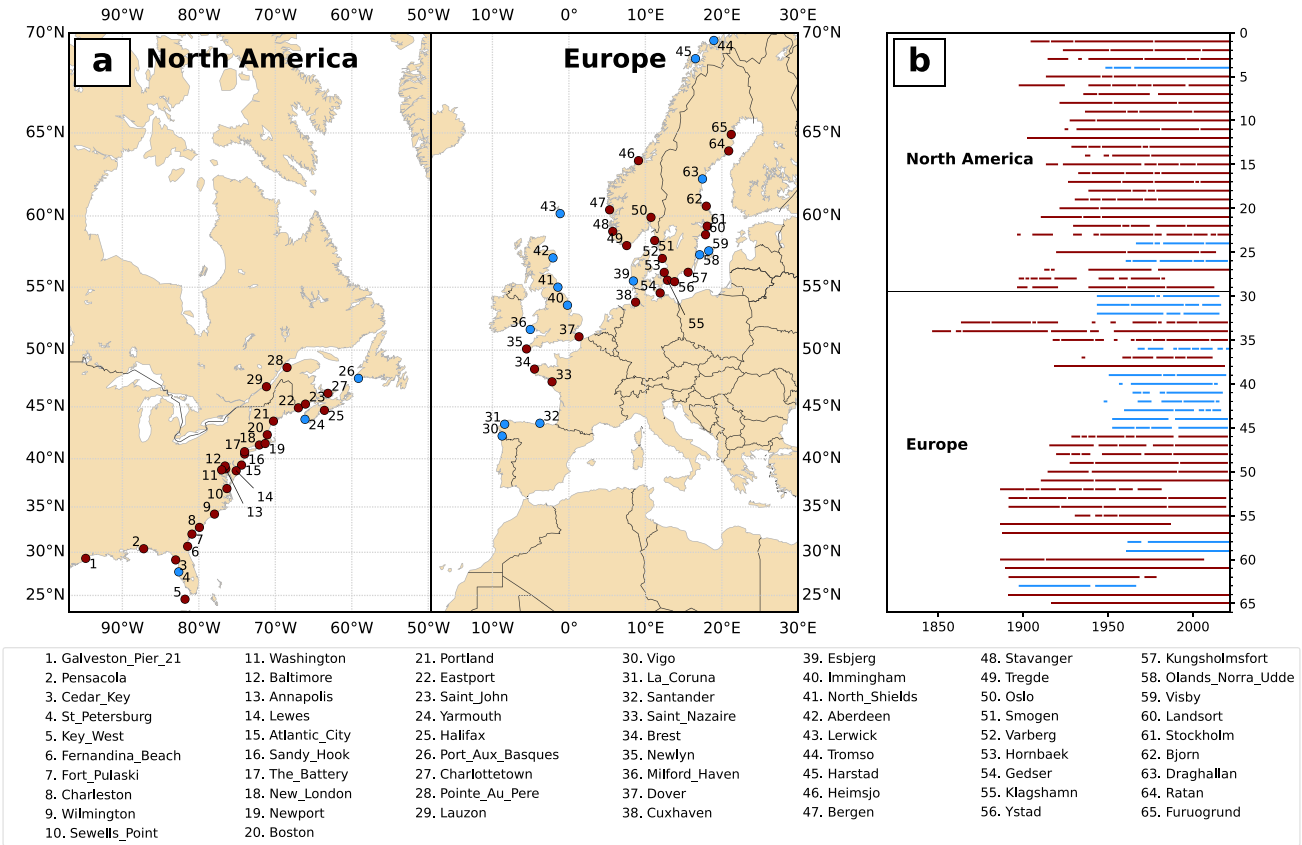

Figure 1. Tide gauges from GESLA-3 data set (a) localization (b) timeline of the data availability. Tide gauges with more than 80 years of data are in red, those between 50 and 80 years are in blue.

All peak surges selected as a storm surge event have been visually controlled to assess their validity and some suspicious measurements were systematically removed (complete list in Table S1). Most of them occur before 1970 and are likely to be standard errors of analogue tide gauges: singular peaks, clock offset, elevation offset (Pugh & Woodworth, 2014).

2.2. Atmospheric Data

The atmospheric data are extracted from the ERA5 reanalysis (Bell et al., 2021; Hersbach et al., 2020) from 1979 to present. Atmospheric pressure and wind speed are extracted at the closest sea point of the grid for each tide gauge. Note that the tide gauges Pointe-au-Père, Varberg, Ystad, Bjorn and Draghallan (stations 28, 52, 56, 62 and 65) have very few data after 1979, thus no extraction can be done at these locations and the atmospheric properties associated with the peak surge will not be analyzed for these stations (i.e., atmospheric data are not plotted further on Figures 8b–8e and 9c).

3. Methods

The analysis of the storm surge events is based on the ECHAR method (Event CHARacterization; Pineau-Guillou et al., 2023), which helps characterize the full dynamics of the storm surge events.

Basically, we characterize events occurring n times per winter (here, $n = 5$), with a classical $72h$ independence criterion (Marcos & Woodworth, 2017; Pineau-Guillou et al., 2023). The independence criterion ensures that each maximum corresponds to a single storm event. For each event, we extract the surge elevation from 20 days before to 20 days after the peak surge. We chose 40 days, because storm surge events mostly last less than 40 days in the North Atlantic (see further details in the Results section).

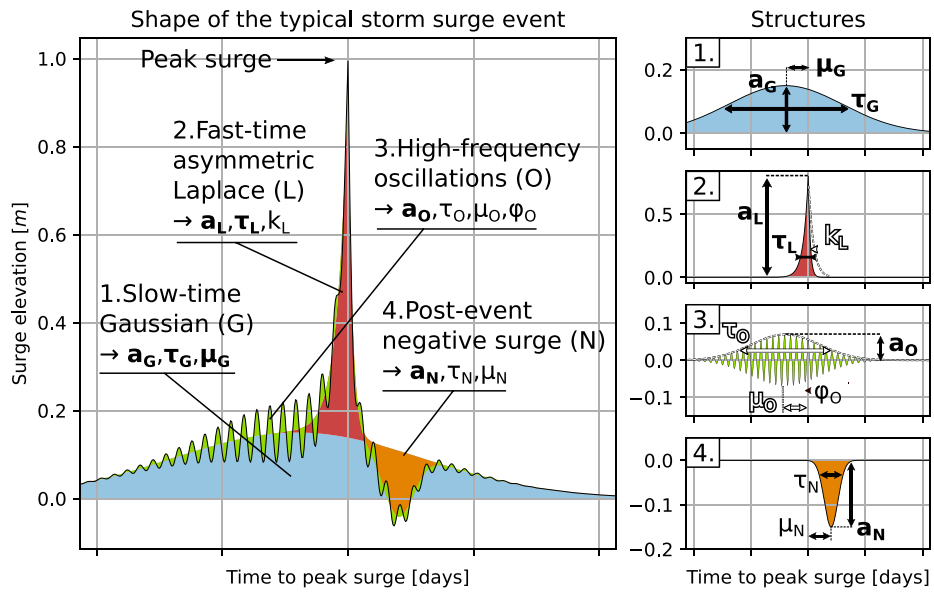

Figure 2. Illustration of the four different structures of the empirical model that fit the typical storm surge shape. The structures are characterized by the amplitude (a), the duration (τ), the delay (μ), the asymmetry (k) and the phase (φ). The bold parameters refer to the characteristic parameters of the storm surge shape and the other ones refer to minor parameters.

The ECHAR method allows the extraction of the typical shape of the extreme events and estimates its different components. The typical shape is computed as the expectation of the surge probability distribution at each hour (see Figure 2 in Pineau-Guillou et al., 2023, for more details). This means that all the events have been stacked to compute the typical storm surge, minimizing the importance of the events that are not like the majority. Thus, the shape of the typical event statistically represents the common shape of the events. Once obtained, the typical shape is then empirically modeled, combining two main structures: a Gaussian slow-time component, mainly induced by the atmospheric pressure, and a Laplace fast-time component, mainly induced by the wind stress.

In the present study, the initial empirical models (i.e., Gaussian and Laplace structure) are modified: the Laplace structure is allowed to be asymmetric and two secondary structures are added to catch possible high-frequency oscillations and a negative surge (Figure 2). The model now expresses as:

$$y(t) = y_G(t) + y_L(t) + y_O(t) + y_N(t) \tag{1}$$

where the slow-time Gaussian structure (hereafter Gaussian structure, subset G), the fast-time Laplace structure with asymmetry (hereafter Laplace structure, subset L), a high-frequency Oscillation structure (hereafter Oscillation structure, subset O) and a post-event Negative surge (hereafter Negative structure, subset N) are defined as:

$$y_G(t) = a_G \exp\left(\left(\frac{t-\mu_G}{2\sigma_G}\right)^2\right) \tag{2}$$

$$y_L(t) = \begin{cases} a_L \exp\left(-\sqrt{2}\ \frac{|t|}{\sigma_L}\right), & if \quad t>0 \\ a_L \exp\left(-\sqrt{2}\ \frac{|t|}{k_L\sigma_L}\right), & if \quad t\le 0 \end{cases} \tag{3}$$

$$y_O(t) = a_O \cos\left(\omega_{M_2} t - \varphi_O\right) \exp\left(\left(\frac{t-\mu_O}{2\sigma_O}\right)^2\right) \tag{4}$$

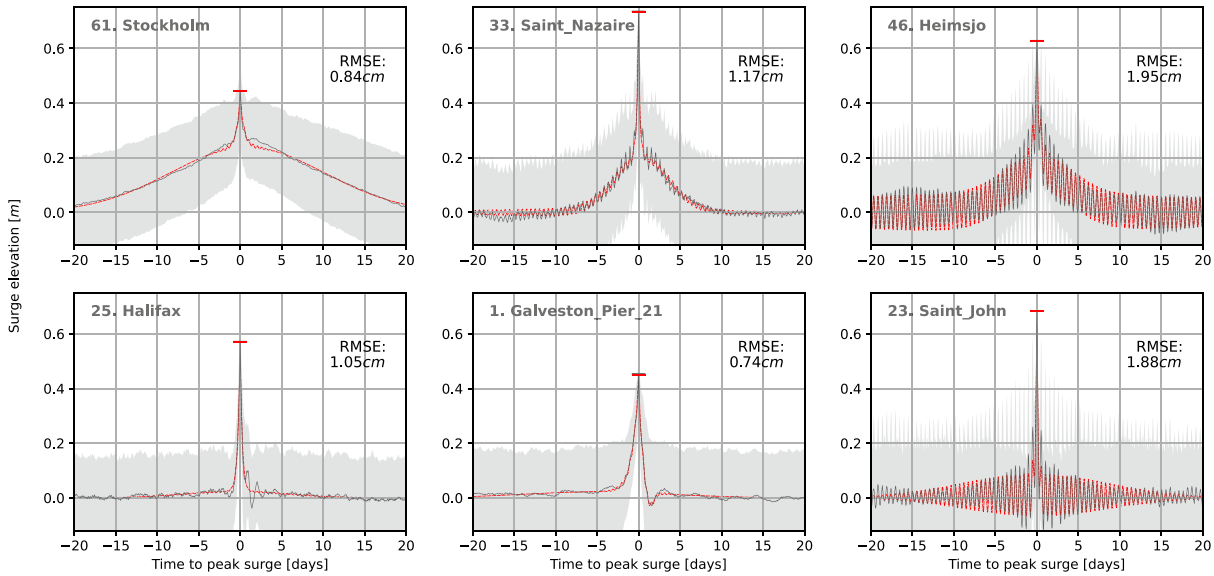

Figure 3. Typical storm surge shape (black curve), its standard deviation (shaded area) and the empirical model fit (red curve) for few tide gauges that represent the diversity of the cases that have been handled. The peak surge elevation is highlighted with the small bar at $t = 0$. All tide gauges typical shapes and fits can be found in Figures A1 and A2.

$$y_N(t) = a_N \exp\left(\left(\frac{t-\mu_N}{2\sigma_N}\right)^2\right) \tag{5}$$

with a the amplitude, μ the delay to the peak surge, σ the standard deviation, k the asymmetry ratio ($k > 1$ refers to steeper slope), ω_{M2} the tidal frequency of M2 constituent (12h25) and φ_O the phase lag of the oscillation.

The structures will first be analyzed through amplitude and duration τ computed as $\tau = 4\sigma$ for the Gaussian, Oscillation and Negative structures and $\tau_L = 2\sigma_L\,(1 + k_L)$ for the Laplace structure (due to the asymmetry). This new model leads to 13 parameters with seven major ones: the amplitude and duration of the Gaussian and Laplace structures (a_G, τ_G, a_L, τ_L), the amplitude of the oscillations (a_O), the amplitude of the negative surge (a_N), and the delay to the peak surge of the Gaussian structure (μ_G), called characteristic parameters (bold symbols in Figure 2). Six minor parameters are also used in the equations but will not be shown here because they do not refer to significant physical processes and are only needed to perform the best estimation of the characteristic parameters.

The fitting method is also updated to evaluate all the parameters with a single fit, using a least squares minimization (Trust Region Reflective algorithm from Scipy Python package). Compared to the previous approach that estimated them sequentially, we estimate all the structures at once using Equation 1. This method improves the estimation of the Gaussian and Laplace structures, especially for the tide gauges with a strong Oscillation or large Negative structures. Because of the high number of parameters (13), the fit needs additional constraints to be sufficiently stable: range, prior and weight. Firstly, the range and the prior (i.e., initial value) are fixed for each parameter (see columns 3 and 4 in Table A1). Secondly, as the fit covers ±20 days around the peak surge, we set a weight to increase the importance of fit near the peak surge (roughly ±5 days). The weighted function is defined with a Gaussian and Laplace function (Figure S1) to be close to the expected typical shape of the event in Pineau-Guillou et al. (2023). We checked that this weighted function increased the performance of the fit in both North American and European coasts. In several European tide gauges, the fit stability is still poor when the four structures are fitted together: the Laplace and Negative structures strongly overlap each other which provokes an overestimation of these two structures' amplitude. However, as in Europe there is almost no negative surge after the peak surge, only the three structures of Gaussian, Laplace and Oscillation are fitted for all European tide gauges. The accuracy of each parameter estimation is evaluated by looking at the increase in the RMSE of the fit when changing a single parameter from the optimal fit. Structures with a significant amplitude (i.e.,

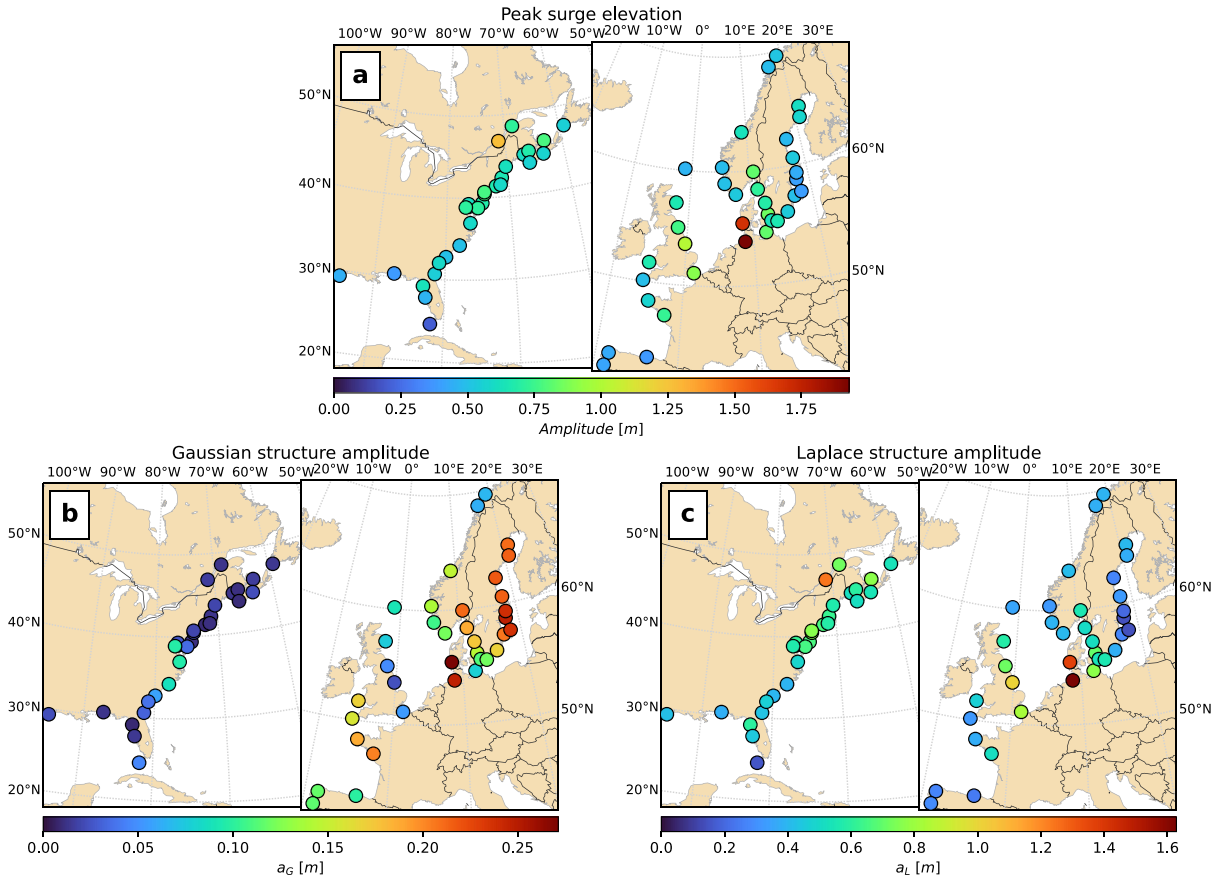

Figure 4. Amplitude of the typical storm surge event: (a) classical peak surge elevation approach, (b) ECHAR Gaussian structure and (c) ECHAR Laplace structure. As all the structures have different ranges of amplitude, upper limits are set independently on subplots (a–c).

greater than 5% of the peak surge) are accurately estimated, whereas for the others, the duration and lag parameters are not as accurately determined, but this has a minimal impact on the results.

4. Results

The improved ECHAR method was applied on the 65 tide gauges. The shape of typical storm surge events was successfully modeled (see some examples in Figure 3, and all tide gauges in Appendix Figures A1 and A2). The RMSE of the empirical model fit is very small with an average between all the tide gauges of 1.3 ± 0.6 cm (against 2 cm in previous ECHAR version) and a maximum of 3.6 cm (against 4 cm in the previous ECHAR version). The largest values of the RMSE are explained by the presence of very singular structures at some tide gauges (e.g., the pre-event negative surge at Immingham on Figure A2) which were not considered by the empirical model. The difference at the peak surge between the model and observation is highly reduced by construction (due to the weight during the fit to catch the observed peak surge); the absolute average difference is of 0.2 ± 0.2 cm and up to at 1.2 cm at Lauzon (station 29 in Saint Lawrence estuary).

The spatial variability of characteristic parameters is first presented for the main structures (Gaussian and Laplace) and then for the secondary ones (Oscillation and Negative).

4.1. Main Structures: Gaussian and Laplace

The spatial variability of the Gaussian and Laplace amplitude (a_G and a_L) is compared to the standard metric of storm surge: the peak surge elevation (Figure 4). As a reminder, the Gaussian structure is mainly driven by the atmospheric pressure, whereas the Laplace one by the wind stress (Pineau-Guillou et al., 2023). Focusing on the peak surge (Figure 4a), only a few tide gauges (6 among 65) show exceptional amplitude compared to the others:

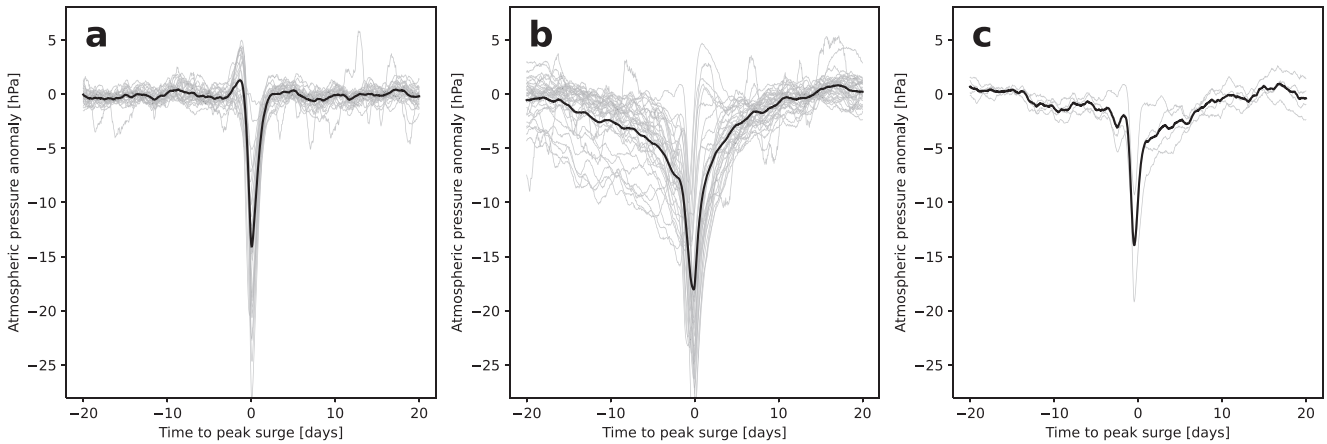

Figure 5. Typical shapes of atmospheric pressure anomaly during storm surge events at the tide gauges of (a) North America coast, (b) European coast and (c) United Kingdom east coast. The gray lines refer to the typical shape at each individual station and the black line refers to the mean shape (station averaged).

they are located in the North Sea (Cuxhaven and Esbjerg, stations 38 and 39, with more than 1.5 m; Dover and Immingham, stations 37 and 40, with around 1 m), and along the St. Lawrence River (Lauzon, station 29, with around 1 m). Focusing on a_L (Figure 4c), the spatial pattern is similar to the one of the peak surge elevation. This strong contribution of the Laplace structure to the peak surge was already reported for the North Sea, where the shallow bathymetry enhances the impact of the wind stress over the atmospheric pressure (Pineau-Guillou et al., 2023). This explanation is plausible for the St. Lawrence and New York bays as well. Note that no significant amplitude is observed in the Baltic Sea, the south of Bay of Biscay and the north of Europe as the bathymetry rapidly reaches 100 m. The spatial pattern of a_G (Figure 4b) really differs from the one of the peak surge elevations and is clearly contrasted between North America, where the Gaussian structure is almost null, and Europe, where a_G is of around 15 cm everywhere. Note a few exceptions: in North America, significant amplitude at Washington (station 11; 8.3 cm) and the coasts of Georgia (stations 6–9; around 7 cm), whereas in Europe very small amplitude on the Eastern coasts of the United Kingdom (stations 37, 40–43; lower than 4 cm).

The absence of Gaussian structure in North America is fully explained by the shape of atmospheric pressure events (Figure 5). As the storm surge Gaussian structure is driven by the atmospheric pressure, the typical shape of the atmospheric pressure corresponding to the selected storm surge events was computed with ECHAR. Typical shapes for North America, Europe and the eastern UK tide gauges are shown respectively in Figures 5a–5c. The difference of winter storm atmospheric pressure shapes across the North Atlantic is clear: there is no Gaussian structure in North America. The atmospheric pressure along the eastern UK also displays a Gaussian structure weaker than other locations in Europe (Figure 5b), explaining the weak value of a_G along these coasts (Figure 4b).

After the amplitude, we now focus on the duration of Gaussian and Laplace structures (Figure 6), keeping in mind their respective amplitude (see the size of the circles on Figure 6). In Europe, the Gaussian duration τ_G is well regionalized with three main areas: the Bay of Biscay and the North Sea (15–20 days), the northern Norwegian fjords (around 30 days) and the Baltic Sea (35–40 days). At the Baltic Sea entrance, we observe a sharp increase of the Gaussian duration: the Gaussian duration lasts 21 days at Hornbaek (station 53, in blue on Figure 6) and 32 days at Klagshamn (station 55, in orange on Figure 6), whereas these two stations are very close (around 120 km between them). In North America, there is almost no Gaussian structure.

Overall, the duration of the Laplace structure (2.7 days in average) is way shorter than the Gaussian one (24.2 days in average). The Laplace structure duration is also regionalized for both North American and European coasts. In North America, the Laplace structure is longer south of New York Bay (stations 1–17; 3.3 days in average) and shorter north of it (station 18–29; 1.6 days in average). In Europe, there is four distinct areas of Laplace duration: long along Spain coasts (stations 30–32; 4.2 days), very short along French and UK coasts (stations 33–37 and 40–42; 1.3 days in average), short in the North Sea and the Baltic Sea (stations 38–39 and 46–65; 2.8 days in average) and very long in the northern Norwegian fjords (stations 44–45; 5.8 days in average).

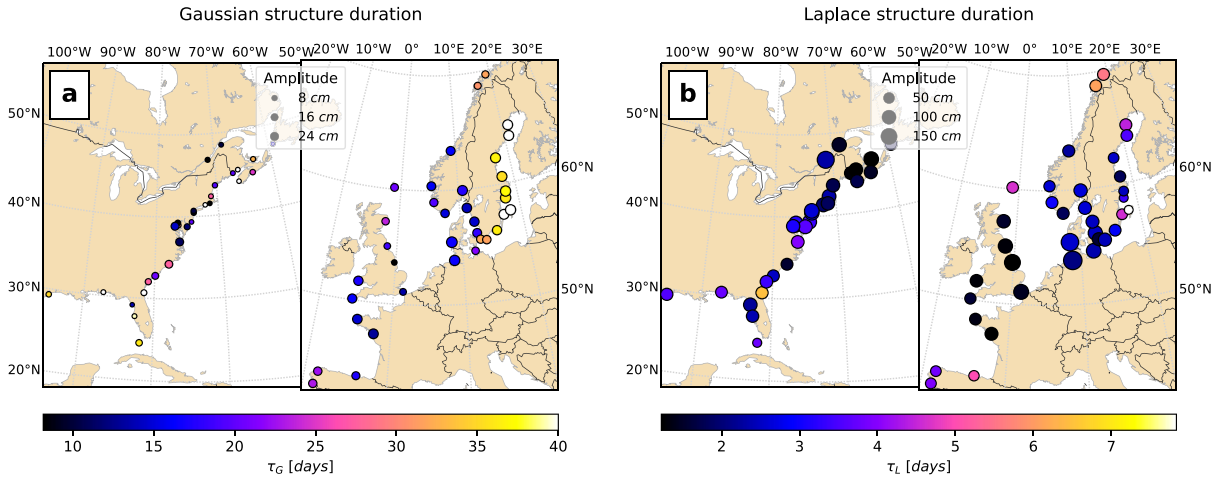

Figure 6. Duration of the typical storm surge event: (a) Gaussian structure, (b) Laplace structure. The size of each tide gauge is related to the amplitude of the structure.

4.2. Secondary Structures: Oscillation and Negative

After describing the main structures of the typical storm surge shape, secondary structures are now analyzed. The Oscillation structure catches high-frequency oscillations at M2 frequency (12h25; see Figures 2 and 3 for the illustration). In the North Atlantic, only 13 tide gauges among 65 have an Oscillation structure larger than 4 cm (Figure 7a). These stations are located in the Bay of Fundy, at Washington, along the North Carolina coasts, in the northwest fjords of Norway and Oslo, in the southeast of the North Sea, in the English channel and in the south of the Bay of Biscay. These oscillations are mainly the signature of tide-surge interaction.

The tide-surge interactions result from a combination of the tidal range, the bathymetry, the bottom roughness and the surge amplitude (Idier et al., 2019). Thus, it is quite hard to obtain a single criterion that could explain the observed large oscillation amplitude at some tide gauges. Most of these stations are located in shallow waters, except for Heimsjo (located in a Norwegian fjord; station 46), the North of Spain (close to the shelf break; stations 31 and 32) and the Bay of Fundy (where the isobath 150 m is located within 50 km the coast; stations 22 and 23). Their tidal range and surge amplitude vary between 1.5–6 m and 0.3–1.8 m, but other tide gauges present similar ranges without tide-surge interaction. The amplitude of the Oscillation structure found in this study is quite similar to the tide-surge interaction amplitude found in the simulations of the North Sea (Horsburgh & Wilson, 2007; Idier et al., 2019) and in tide gauge records (Mawdsley & Haigh, 2016). But as the

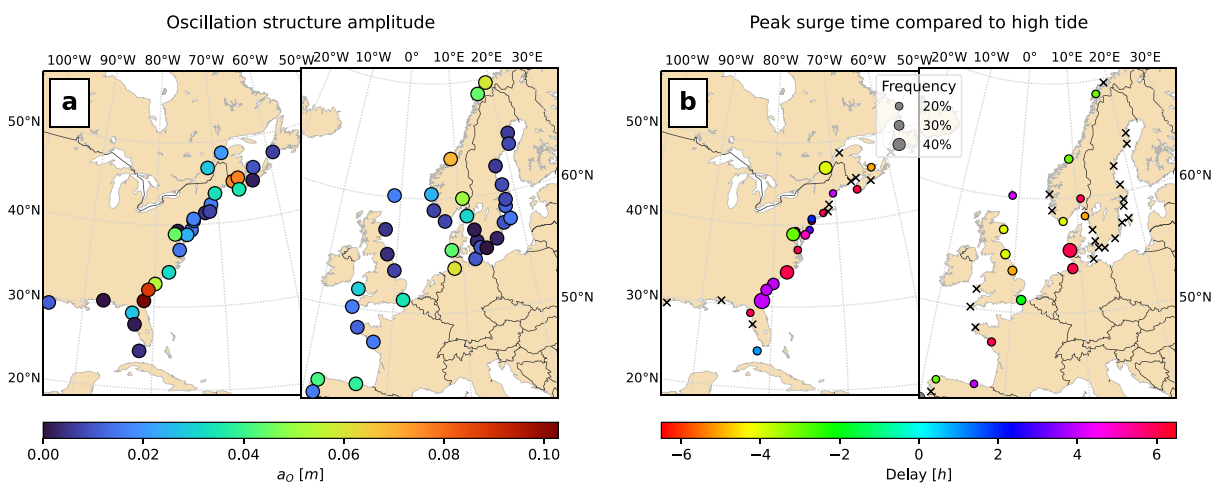

Figure 7. (a) Amplitude of the ECHAR Oscillation structure. (b) Delay of the peak surge with regard to the high tide. The value of the delay refers to the 1h interval where the frequency of peak surge (in %) is maximum; frequency which is proportional to the size of the points. Crosses correspond to insignificant values, that is, where the frequency of all intervals are smaller than 15%.

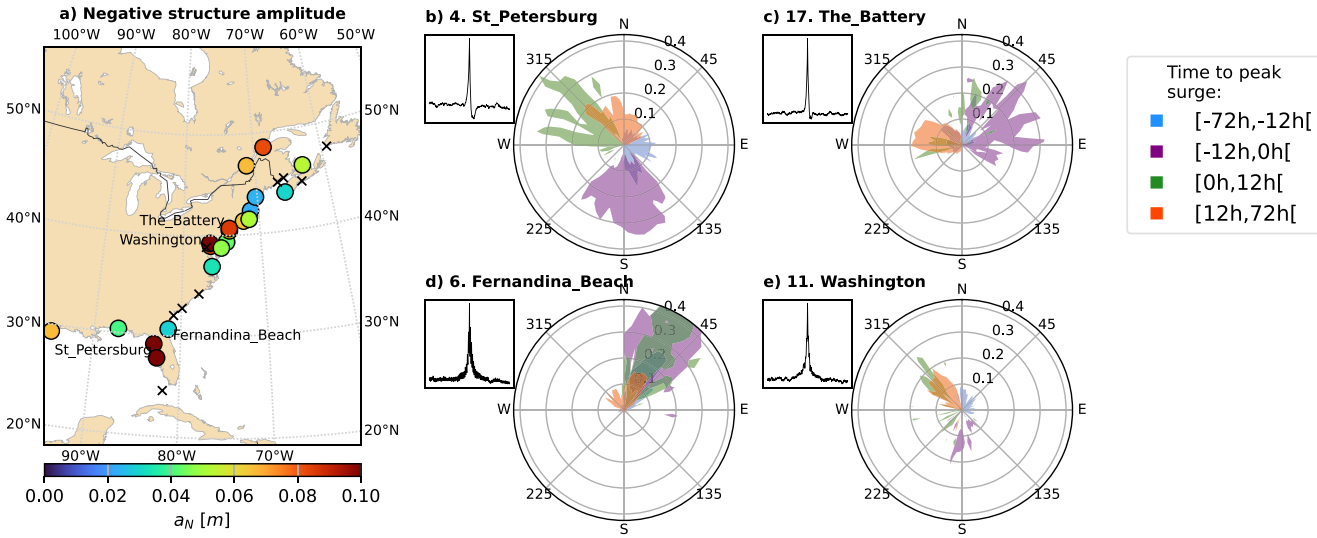

Figure 8. (a) Amplitude of ECHAR Negative surge structure. Crosses correspond to tide gauges without such structure. Note that the North-East Atlantic is not represented, as this structure is not present on the east side of the Atlantic. (b–e) Histogram of wind direction and amplitude before and after the peak surge for tide gauges (a) with a Negative structure and (c, d) without it along the North American coast. The storm surge typical shape of each tide gauge is given at the top left of each subpanel.

tide-surge interactions are estimated with different methods, the results sometimes differ. With simulations, tide-surge interactions are estimated computing the difference between a simulation with tide and atmospheric forcing and a simulation with tide only. With tide gauge records, tide-surge interactions are usually estimated by the difference between the non-tidal residual (instantaneous difference between the observed and predicted sea level) with the skew surge (difference between the maximum observed sea level and the maximum tide prediction during a tidal cycle (Pugh & Woodworth, 2014), even if other methods co-exist (for more details, see Mawdsley & Haigh, 2016). However, all these methods are indirect, whereas in the present study, the amplitude of the tide-surge interaction is directly estimated from the observed oscillations in tide gauges, highlighted thanks to the ECHAR method. For this reason, it is a more accurate way to estimate tide-surge interactions.

Various studies pointed out that the strongest surge events may happen preferentially at a certain stage of the tide (e.g., mid-tide in the English Channel; Haigh et al., 2010; Schmitt et al., 2018). Such consistency suggests that the increased sea level due to the atmospheric surge strongly modifies the tidal propagation, then, the high water being shifted by a few minutes, this leads to oscillations in the surge signal (see Figure 4 of Horsburgh & Wilson, 2007). Similar investigations have been made at every station by computing the histogram of the delay between the peak surge and the high tide. The mode of this histogram (i.e., the highest peak) and its frequency (i.e., the number of values at the highest peak, expressed in %) is shown in Figure 7b. Note that as we have 12 classes of 1h, as soon as the frequency of all the intervals are smaller than 15%, the recurrent tide period is not significant.

We found that 34 tide gauges (i.e., nearly half of the tide gauges) have significant tide delay, that is, strong tide-surge interaction. Which can explain some of the large oscillations despite a small tidal range (stations 6–9 along the Georgia coasts, Washington, Lauzon and Esbjerg, stations 11, 29, 39 on Figures 7a and 7b). However, it cannot explain the large oscillations at the Bay of Fundy (large oscillations on Figure 7a, but no tide delay on Figure 7b), that may be mostly due to the large tidal range and where even a small change of sea level can highly modify the tidal propagation. Figure 7b also points out that the tidal delay is very diverse over the North Atlantic and that the surge can happen preferably before high tide, as already observed in the English Channel (Haigh et al., 2010; Schmitt et al., 2018) but also after high tide (e.g., along Georgia coasts). This study does not claim to fully explain this complex interaction and only proposes a new quantification approach.

The seiches can also be responsible for oscillations that can reach 30 cm or more, with a frequency linked to the shape of the harbor and/or the bay where the tide gauge is located from a few minutes to hours (Chrystal, 1906;

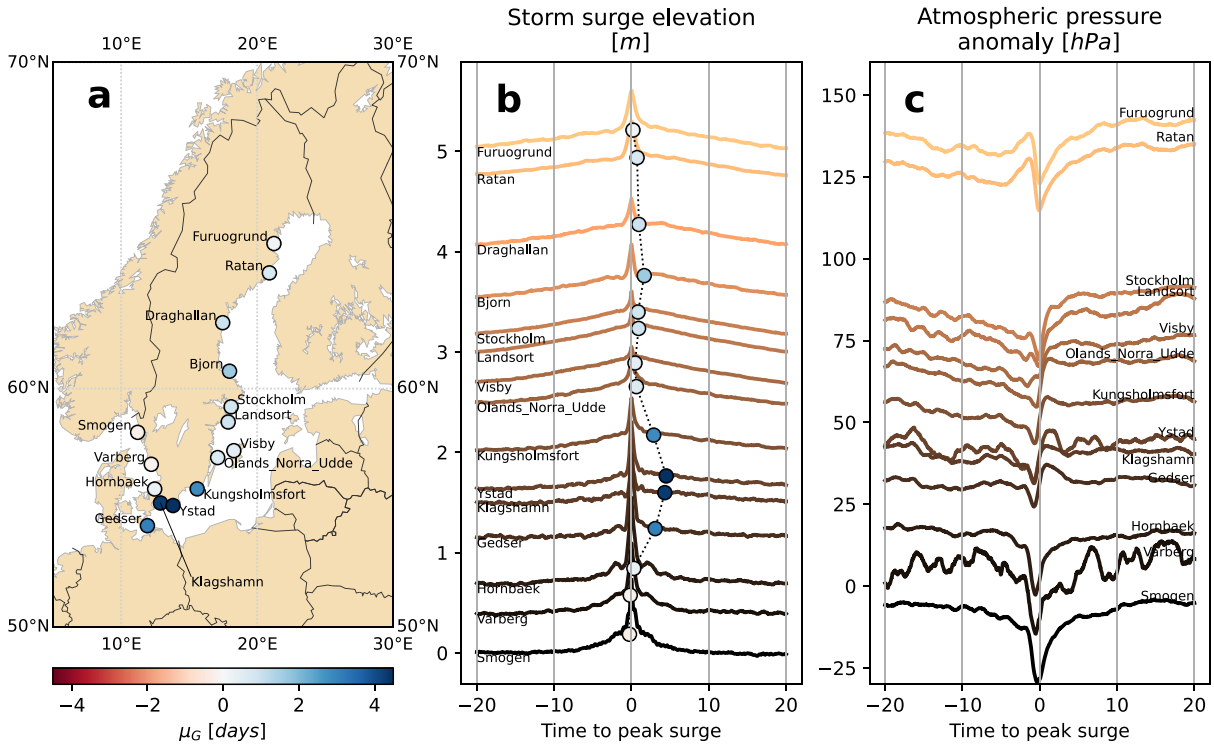

Figure 9. (a) Time lag of the Gaussian structure in the Baltic Sea, and typical shape of (b) the storm surge event (c) the corresponding atmospheric anomaly from the Denmark strait (dark lines) to the North of the Baltic Sea (wheat lines). The circles in panel (b) refer to the center of the storm surge Gaussian structure and their colors refer to the time lag as in panel (a).

Rabinovich, 2009). They may be generated by the action of the wind or infragravity waves (Ardhuin et al., 2010; MacMahan, 2015; Park et al., 2016). Seiches that have a frequency below 2 hr could not have been properly sampled with hourly data and remain a residual noise in the surge signal. Seiches with larger frequency could sign in the data with oscillations at the frequency of the basin/harbor. However, we did not find any tide gauge that shows oscillations at other frequencies than the M2 one in the typical events (Figures A1 and A2). Possibly seiches occur only occasionally, depending on atmospheric and oceanic conditions, and thus do not impact the typical shape of storm surge events. Further investigations would be needed to discriminate the tide-surge oscillations from the seiches in the bays, where the resonant frequency is around the tidal one.

After analyzing the Oscillation structure, we now move to the Negative structure. This Negative structure corresponds to a small but significant negative surge, which occurs at some tide gauges just after the peak surge (see Figures 2 and 3 for the illustration). The tide gauges with strong negative surge ($a_N > 5$ cm) are located in very specific areas (Figure 8a): in the Gulf of Mexico (stations 1–4), along the coasts from Baltimore to Boston (stations 12–19) and in the narrow water bodies of the Saint Lawrence Bay (stations 27–29).

Analyzing the wind data, it appears that the wind direction is turning during the storm event, causing the Negative structure. Indeed, the histograms of the wind direction were computed for all the selected events during four periods around the peak surge ([−72h, −12h], [−12h, 0h], [0h, 12h] and [12h, 72h], 0h referring to the peak surge). Note that the histograms of each period were extrapolated over the entire [−72h, 72h] and normalized by the number of events, to obtain comparable density between the periods and tide gauges.

The results at four tide gauges are presented in Figure 8b–8e. At St Petersburg (station 4; Figure 8b) and The Battery (station 17 near New York; Figure 8c), where a significant Negative structure is observed, the gradual shift of the wind direction before and after the peak surge is clear: at St Petersburg (Figure 8b) the wind comes from the east, then from the south before the peak surge moving to west-northwest, then north wind after the peak surge, at The Battery (Figure 8b) the wind comes from east-northeast before the peak surge moving to

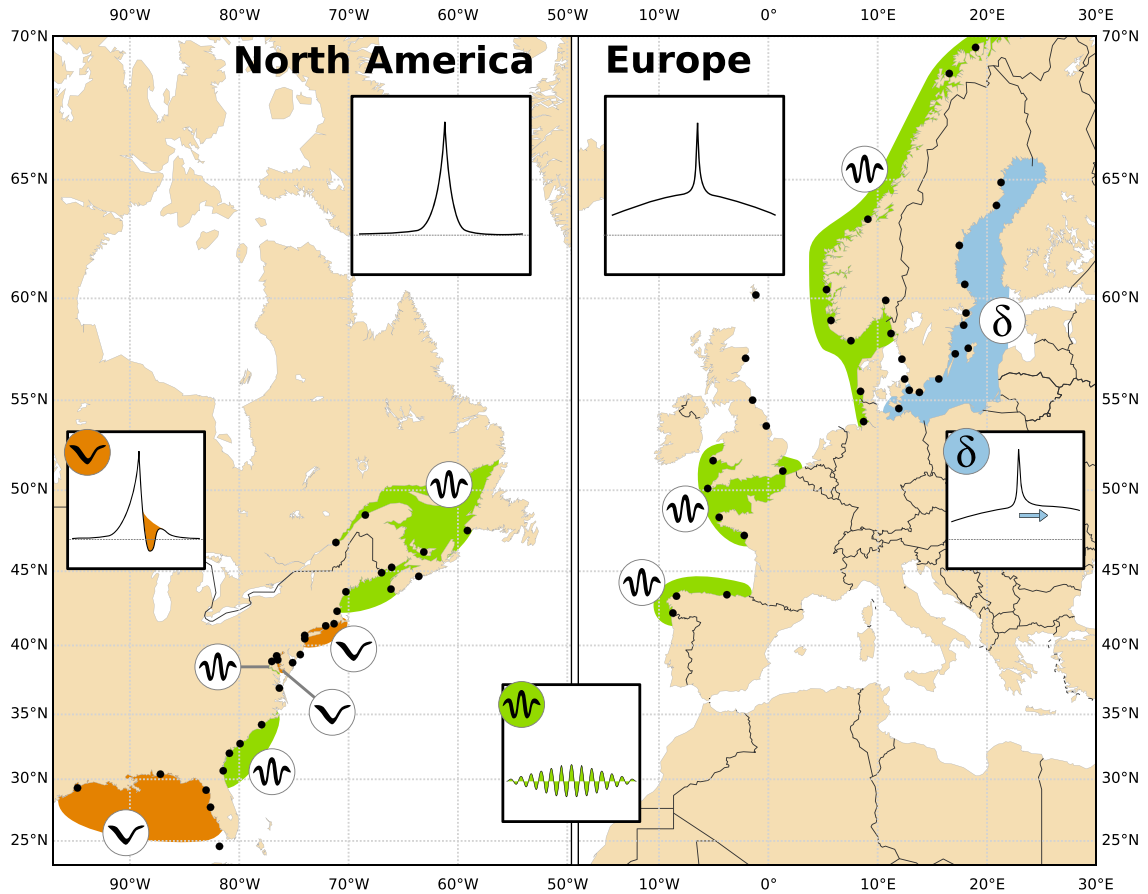

Figure 10. Synthesis of the spatial variability of the typical storm surge events in the North Atlantic tide gauges. Europe displays a Gaussian and Laplace structure, whereas North America mainly displays a Laplace structure (see the two illustrations at the top of the figure). In addition, we may observe: a Negative surge just after the peak surge (in orange), a delay in the Gaussian structure (in blue, mainly in the Baltic Sea), some oscillations due to tide-surge interaction (in green).

northwest-west wind after the peak surge. Thus, before the peak surge, the Ekman transport due to the wind pushes the water toward the coasts. On the contrary, after the peak surge, the changing direction of the wind leads to an Ekman transport that pushes the water away from the coasts, generating a Negative surge structure. Note that within the 2 days after the peak surge, the atmospheric pressure is still contributing to the rise of the sea level (Figure 5a), so the impact of the wind stress needs to be strong enough to surpass it and form a negative surge.

Finally, we also investigated the evolving wind direction, at tide gauges without significant Negative surge (Fernandina Beach and Washington, stations 6 and 11, Figures 8d and 8e) where two different wind conditions are observed. At Fernandina Beach, the wind has the same direction (northeast wind) during the entire storm surge event (Figure 8d), whereas at Washington, there is no specific wind direction before the peak surge (blue and purple in Figure 8e) with weaker wind speed that cannot surpass the elevation due to the atmospheric pressure. To conclude, a changing wind direction during the storm event may lead to the presence of a Negative structure. However, analyzing deeply all tide gauges, some exceptions were found at 2 tide gauges among 65: at Halifax and Port-aux-Basques (stations 25–26, Canada), a strong wind direction inversion is observed during the typical storm surge event, but no significant Negative structure is found in its typical storm surge shape (see in Figure 3). As already mentioned above, the impact of the wind stress must be strong enough to surpass the atmospheric pressure effect (which generates a positive surge). However, the proximity of the shelf break near Halifax and Port-aux-Basques explains the lower impact of the wind at this location, as the wind stress is not strong enough to surpass the atmospheric pressure effect.

4.3. Delayed Gaussian Structure Within the Baltic Sea

The Baltic Sea has a very specific typical shape of storm surges (see for example Stockholm on Figure 3). Whereas at most stations, the Gaussian structure is centered on the peak surge (e.g., Saint-Nazaire on Figure 3), in the Baltic Sea, we observe a strong time lag between the maximum of the Gaussian and the peak surge (μ_G, see Figure 2 for the illustration). The Gaussian structure time lag varies from the Denmark straits to the northern part of the sea (Figures 9a and 9b). In the South, at the two entrances of the Baltic Sea (Gedser and Klagshamn) μ_G is the strongest, with a lag of almost 4 days after the peak surge. Moving to the north, μ_G decreases until the middle of the Baltic Sea (Visby and Olands Norra Udde), and then increases again in the northern part. As the Gaussian structure is linked to the atmospheric pressure, the typical shape of the corresponding atmospheric pressure is shown in Figure 9c. The typical shape of the atmospheric pressure that leads to the strongest storm surge is clearly different between the tide gauges located before the Denmark straits (Smogen, Varberg and Hornbaek) and after. Inside the Baltic Sea (i.e., from Gedser to Stockholm), the atmospheric pressure increases drastically just after the peak event, reaching levels even higher than at the beginning of the event. Such high atmospheric pressure levels may induce a sea level drop which will mitigate the wind effect in the Baltic Sea. Instead, the Gaussian structure still increases after the peak surge and shows the longest duration of the North Atlantic (see Figure 6). Stanev et al. (2018) quantify the inflow and outflow at the entrance of the Baltic Sea highlighting specific periods of unbalanced flow that may contribute to the surge dynamics. But to this day, no study explains this dynamic and a dedicated ocean-atmosphere numerical modeling of the Baltic Sea and its entrance during a storm event should help to isolate the mechanisms at stake.

5. Discussions

The ECHAR method allows the extraction of a typical storm surge event shape, from a large number of extreme storm surge events. In the North Atlantic, specific patterns are investigated and the analysis of associated environmental conditions (i.e., tide, atmospheric circulation) allows us to understand the conditions that led to such specific patterns.

Figure 10 summarizes the spatial distribution of the main patterns that have been quantified in this study. In the North Atlantic, we found three wide regions with similar patterns: North America, Western Europe and the Baltic Sea. In North America, the storm surge event is characterized by the absence of a Gaussian structure whereas in Europe, the Gaussian structure is present with an average amplitude of 15 cm (schematic subplots at the top of Figure 10). In the Baltic Sea, the Gaussian structure is delayed, with a maximum occurring up to 4 days after the peak surge (see the blue pictogram δ on Figure 10). Finally, in addition to these basin-scale patterns, we may observe locally some oscillations (see the green pictogram on Figure 10), and sometimes, the presence of a negative surge whose amplitude is of around 6 cm happening around 1.6 days after the peak surge (see the orange pictogram on Figure 10).

The different patterns of storm surge events across the North Atlantic are explained by the different features of storms, between North America and Europe. The extratropical storms occurring in the North Atlantic are created from the orography of the Rocky Mountains (Brayshaw et al., 2009), the distance scale between the low- and high-pressure pole being quite small. As the storm system travels eastward, it can lead to the breaking of a Rossby wave, when the scale distance between the low- and high-pressure pole becomes large enough (Priestley et al., 2017). By classifying the atmospheric pressure patterns, Priestley et al. (2020) obtained the distribution of the different storm families over the North Atlantic. In storm families, primary storms are pre-existing storms, whereas secondary storms are those that form on the trailing front of a primary storm. The North American coasts are preferably impacted by primary storms with small spatial extensions, whereas European coasts are preferably impacted by secondary storms, with larger spatial extensions. Consequently, in North America, tide gauges located along the storm track will be affected by both sides of the cyclonic storm, that is, by the winds turning from one direction to another, leading to a negative surge. Very differently, the European coasts being preferably impacted by large scale secondary storms, tide gauges that may be far from the storm center are generally affected by strong fronts, with large-scale low-pressure anomalies, leading to the presence of a long Gaussian structure in the storm surge event shape.

Although we only focus on extratropical cyclones in the present study, note that in North America, the typical wind fields of the storms present some similarities with the one of tropical storms, that is, the same small spatial

extension. Interestingly, a feature like negative surges just after the peak surge were also reported for tropical cyclones. Liu et al. (2020) simulated storm surges during Hurricane Sandy, on 30 October 2012, along the U.S. East Coast, and reported a strong drop just after the peak surge. Investigating synthetic and modified historical storms, Peng et al. (2006) and Sebastian et al. (2014) both investigated the asymmetry of the surge event when the cyclone hits the coast. They reported a sudden drop of the sea level just after the peak surge for tide gauges at the right side of the cyclone.

Several studies show that storms may occur consecutively, that is, separated by a few days, as in UK winter 2013–2014 (Masselink et al., 2016). Because the ECHAR method is based on a 40-day time analysis, we can wonder if consecutive storms may affect the typical shape of a storm surge event. In fact, two cases are possible. (a) If these consecutive events happen only occasionally (e.g., only during the 2013–2014 UK winter), they will not affect the shape of the typical storm surge event. Indeed, all the events are stacked to compute the typical storm surge shape, minimizing the importance of the events that are not like the majority. (b) On the contrary, if stormy events always co-occur at approximately the same interval (e.g., if storms always come every 3 days), this pattern could affect the shape of the typical storm surge event. Another smaller peak surge may appear before or after the central peak surge. However, we did not find such a configuration in the typical shape of storm surge events (Figures A1 and A2), suggesting that consecutive storms may happen occasionally, rather than systematically, in the locations we investigated.

Concerning the limitations of the method, despite our efforts to focus on extratropical cyclones only (selecting winter data between October and March), a few tropical cyclones that happen in late October are still included in the selected extreme events at a few tide gauges. However, as we stack all the extreme events together, the weight of a few tropical storms over a few hundred events is very low and will not modify the typical shape of the event. Note that using a database of tropical cyclones, such as HURDAT2 (https://www.aoml.noaa.gov/hrd/hurdat/Data_Storm.html) for the U.S. coasts or IBTrACS globally (Knapp et al., 2010), could help to properly distinguish tropical cyclones from extratropical storms and produce distinct typical storm surge events for these two classes.

In perspective, the ECHAR method could be useful to investigate the evolution during the last century of the different contributions to the surges (slow-time Gaussian and fast-time Laplace structures), whereas most previous studies focus on the evolution on the peak surge (Calafat & Marcos, 2020; Dangendorf et al., 2014; Marcos & Woodworth, 2017; Wahl & Chambers, 2015, 2016), which integrate all the different contributions (i.e., atmospheric pressure and wind stress). Using long tide gauges records (e.g., more than 100 years) and a 20- or 30-year sliding window, one could investigate the evolution of the different parameters over time.

Another perspective from the present study is to improve natural hazard risk assessment in coastal areas. Modeling studies for flood and erosion risk need synthetically generated storm surge events, with statistics close to those of observations, as boundary conditions (e.g., MacPherson et al., 2019; Wahl et al., 2011). The ECHAR time series of typical storm surge events (Figures A1 and A2) could be used directly as inputs for such numerical models and associated uncertainties can also be exploited (shaded areas on Figures A1 and A2). Note that all these values are given numerically in Table S2 (typical shape of storm surge events, associated uncertainties and fit) and Table S3 (characteristic parameters of the fit), so that anyone can use these realistic shapes of time-varying storm surges.

6. Conclusion

In the present study, we improved the ECHAR method that was previously used to characterize the storm surge events in Europe (Pineau-Guillou et al., 2023). Initially, storm surge events were modeled with two major structures, a slow-time Gaussian one due to atmospheric pressure lowering and a fast-time Laplace one due to the wind stress. The model was improved to better catch some specific patterns of storm surge events: (a) a possible asymmetry of the Laplace structure (e.g., Galveston Pier): (b) the presence of a negative surge occurring after the peak surge, at some stations in North America and (c) high-frequency oscillations. We analyzed 65 long-term tide gauges over the North Atlantic, and quantified the characteristics of the different structures, in terms of amplitude duration, and delay. This approach enriches the description of the extreme events and highlights spatial coherence that might have been missed, when analyzing only the peak surge (i.e., the maximum value of the surge).

The main differences in typical shapes are observed between North America and Europe, because of the absence of the slow-time Gaussian structure in North America, whereas in Europe, its amplitude is of around 15 cm and its duration around 24 days (18 days outside the Baltic Sean and 32 days inside). This absence of Gaussian structure in North America is explained by a smaller spatial extension of the extratropical storms, with a more localized atmospheric pressure drop. The Baltic Sea also shows a unique pattern of delayed (up to 4 days after the peak surge) and extended (duration around 32 days) Gaussian structure with no trivial explanation. No particular differences of the fast-time Laplace structure were observed between North America and Europe; its amplitude is of around 53 cm and its duration of around 1.4 days.

Secondary structures are also added in the ECHAR model, which highly reduces the RMSE (average of 1.3 cm, against 2 cm in previous version). First, coherent regions with a negative surge occurring just after the peak surge are highlighted along the North America coasts. This negative surge occurs around 1.5 days after the peak surge, with an amplitude of around 6 cm. Such sudden drop of the sea level is explained by turning winds and storms of smaller extent in North America, compared to Europe. Second, high-frequency oscillations, with amplitudes of around 3 cm and up to 25 cm, are observed at specific stations. Such oscillations are the signature of tide-surge interaction and occur at a specific phase of the tide (e.g., 2h before the high tide at Washington).

In the future, promising applications of the ECHAR method could highlight the changes that occurred in the last century on the shape of the storm surge events and other processes that could happen during summer storms or in other coasts worldwide.

Appendix A: ECHAR Fits

In this section, further details about the fit of the observed typical event are provided. The Table A1 shows the constraints of the fit for each of the 13 parameters of the ECHAR model: the range and the prior (i.e., initial value). Then, the observed typical event, its standard deviation and the fitted typical event are shown in Figure A1 for North American tides gauges and Figure A2 for European tide gauges.

Table A1
Range and Prior of All the Parameters of the ECHAR Method

Structure	Parameter	Range	Prior	Unit
Gaussian	$\mathbf{a_G}$	[0,5]	0.2	m
$\tau_\mathbf{G} = \mathbf{4}\sigma_\mathbf{G}$	σ_G	[2,100]	3.0	days
	$\mu_\mathbf{G}$	[−10,10]	0.0	days
Laplace	$\mathbf{a_L}$	[0,5]	0.5	m
$\tau_\mathbf{L} = \mathbf{2}\sigma_\mathbf{L}(\mathbf{1} + \mathbf{k_L})$	σ_L	[0,8]	0.8	days
	k_L	[0,5]	1.0	None
Oscillations	$\mathbf{a_O}$	[0,0.5]	0.0	m
$\tau_O = 4\sigma_O$	σ_O	[1,100]	4.0	days
	φ_O	[-π, π]	0.0	radians
	μ_O	[−10,10]	0.0	days
Negative surge	$\mathbf{a_N}$	[−0.1,0]	0.0	m
$\tau_N = 4\sigma_N$	σ_N	[0.5,0.65]	0.5	days
	μ_N	[0.8,4]	3.0	days

Note. Characteristic parameters of the storm surges are shown in bold.

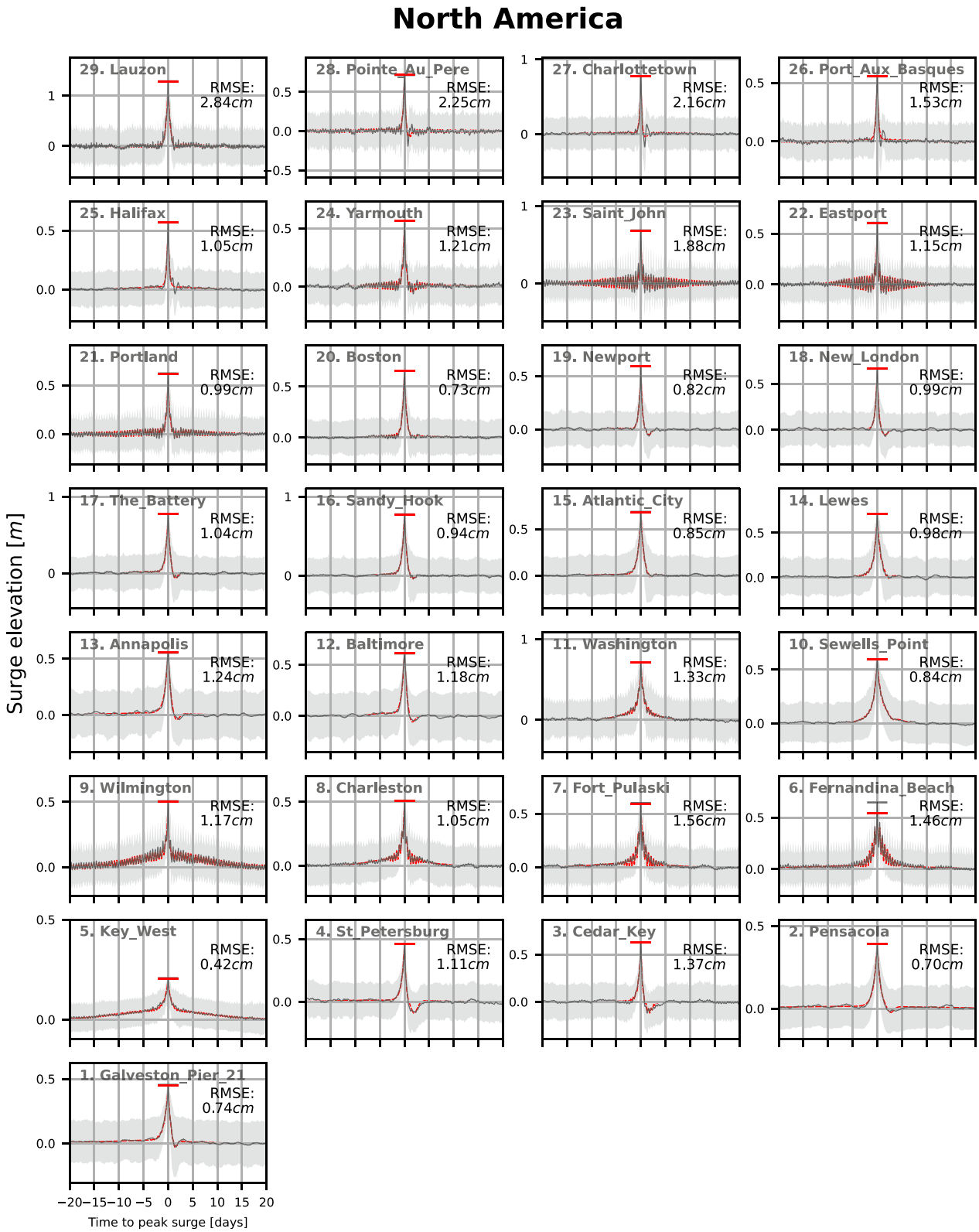

Figure A1. Observed typical shape of storm surges (black line) and the fit of ECHAR model (red line) for all the tide-gauges of the North American coast. The typical shape refers to the statistical shape of the 5 maximum storm surges per winter. The bar refers to the elevation of the peak surge for both observation and the model.

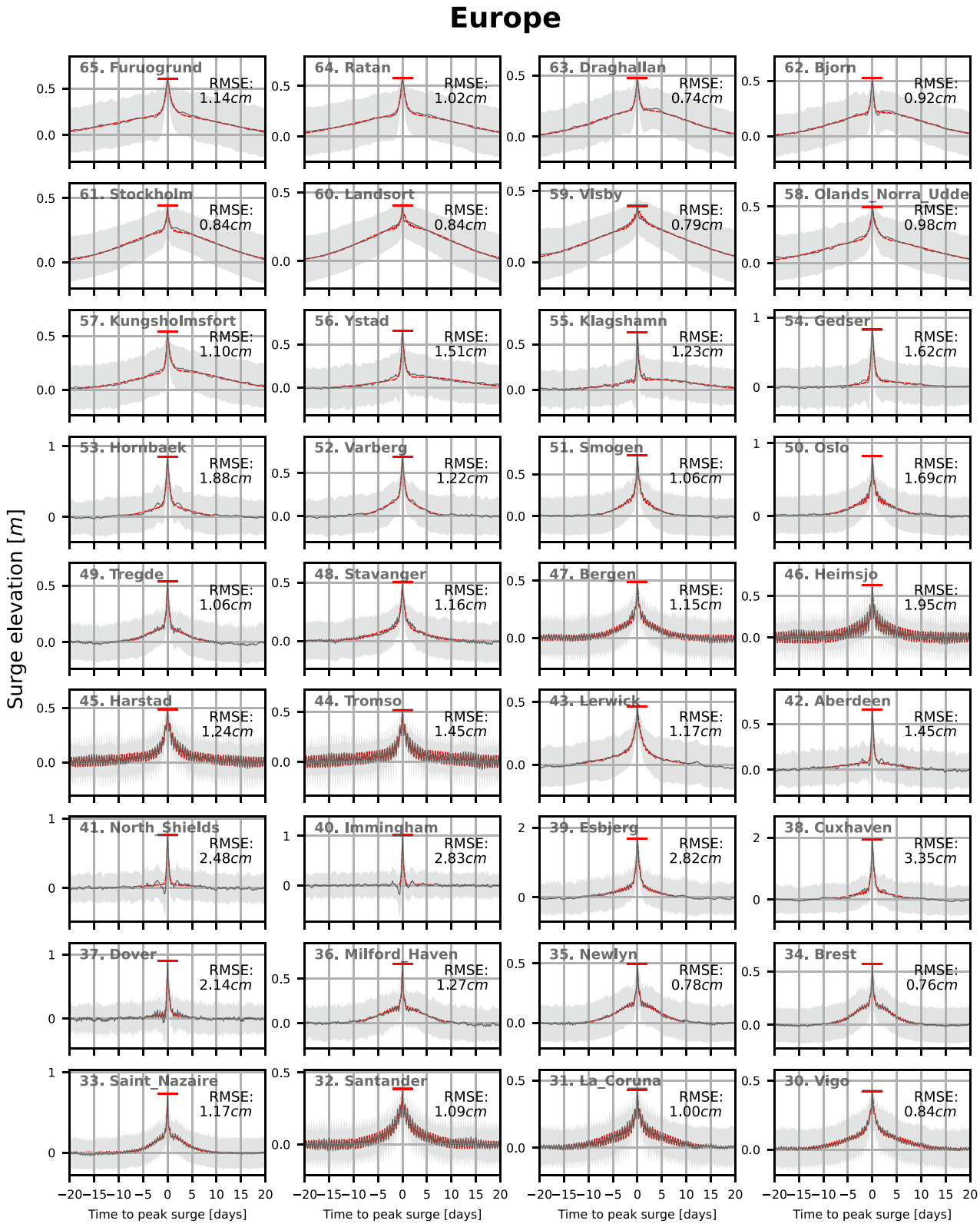

Figure A2. Idem that Figure A1 for tide-gauges along European coasts.

Data Availability Statement

The GESLA data set of tide gauge measurement (Haigh et al., 2022) is available at https://gesla787883612.wordpress.com. The ERA5 global atmospheric reanalysis (Hersbach et al., 2023) is available at https://doi.org/10.24381/cds.143582cf. The Tidal Toolbox (Allain, 2014) can be installed following the instruction at https://si-rocco.obs-mip.fr/other-tools/prepost-processing/comodo-tools/installation/. The suspicious data, the typical shapes, associated variability and the modeled characteristic parameters of the events are available in Supporting Information Tables S1, S2, and S3, respectively.

Acknowledgments
This research has been supported by the French National Research Agency (ANR) Grant ClimEx (ANR-21-CE01-0004).

References

Allain, D. J. (2014). T-UGOm TidalToolbox [Software]. (Technical Report). https://www5.obs-mip.fr/wp-content-omp/uploads/sites/12/2016/10/ttb-1.pdf

Andrée, E., Su, J., Larsen, M. A. D., Madsen, K. S., & Drews, M. (2021). Simulating major storm surge events in a complex coastal region. *Ocean Modelling*, *162*, 101802. https://doi.org/10.1016/j.ocemod.2021.101802

Ardhuin, F., Devaux, E., & Pineau-Guillou, L. (2010). Observation et prévision des seiches sur la côte Atlantique française. In *XIèmes Journées, Les Sables d'Olonne* (pp. 1–8). Editions Paralia. https://doi.org/10.5150/jngcgc.2010.001-A

Baranes, H. E., Woodruff, J. D., Talke, S. A., Kopp, R. E., Ray, R. D., & DeConto, R. M. (2020). Tidally driven interannual variation in extreme Sea Level frequencies in the Gulf of Maine. *Journal of Geophysical Research: Oceans*, *125*(10), e2020JC016291. https://doi.org/10.1029/2020JC016291

Bell, B., Hersbach, H., Simmons, A., Berrisford, P., Dahlgren, P., Horányi, A., et al. (2021). The ERA5 global reanalysis: Preliminary extension to 1950 [Dataset]. *Quarterly Journal of the Royal Meteorological Society*, *147*(741), 4186–4227. https://doi.org/10.1002/qj.4174

Booth, J. F., Narinesingh, V., Towey, K. L., & Jeyaratnam, J. (2021). Storm surge, blocking, and cyclones: A compound hazards analysis for the northeast United States. *Journal of Applied Meteorology and Climatology*. https://doi.org/10.1175/JAMC-D-21-0062.1

Brayshaw, D. J., Hoskins, B., & Blackburn, M. (2009). The basic ingredients of the North Atlantic storm track. Part I: Land–sea contrast and orography. *Journal of the Atmospheric Sciences*, *66*(9), 2539–2558. https://doi.org/10.1175/2009JAS3078.1

Burt, S. D., & Mansfield, D. A. (1988). The great storm of 15–16 October 1987. *Weather*, *43*(3), 90–110. https://doi.org/10.1002/j.1477-8696.1988.tb03885.x

Calafat, F. M., & Marcos, M. (2020). Probabilistic reanalysis of storm surge extremes in Europe. *Proceedings of the National Academy of Sciences*, *117*(4), 1877–1883. https://doi.org/10.1073/pnas.1913049117

Caldwell, P., & Merrifield, M. (2015). Joint archive for sea level. Data Report No. 24. JIMAR Contribution No. 15-392. http://ilikai.soest.hawaii.edu/UHSLC/jasl/datrep/JASL2015DataReport.pdf

Catalano, A. J., & Broccoli, A. J. (2018). Synoptic characteristics of surge-producing extratropical cyclones along the northeast coast of the United States. *Journal of Applied Meteorology and Climatology*, *57*(1), 171–184. https://doi.org/10.1175/JAMC-D-17-0123.1

Chrystal. (1906). On the hydrodynamical theory of seiches. *Transactions of the Royal Society of Edinburgh*, *41*(3), 599–649. https://doi.org/10.1017/S0080456800035523

Cid, A., Menéndez, M., Castanedo, S., Abascal, A. J., Méndez, F. J., & Medina, R. (2016). Long-term changes in the frequency, intensity and duration of extreme storm surge events in southern Europe. *Climate Dynamics*, *46*(5–6), 1503–1516. https://doi.org/10.1007/s00382-015-2659-1

Dangendorf, S., Rybski, D., Mudersbach, C., Müller, A., Kaufmann, E., Zorita, E., & Jensen, J. (2014). Evidence for long-term memory in sea level. *Geophysical Research Letters*, *41*(15), 5530–5537. https://doi.org/10.1002/2014GL060538

Davis, R. E., & Dolan, R. (1993). Nor'esterns. *American Scientist*, *81*(5), 428–439. Retrieved from https://www.jstor.org/stable/29775010

Enríquez, A. R., Wahl, T., Baranes, H. E., Talke, S. A., Orton, P. M., Booth, J. F., & Haigh, I. D. (2022). Predictable changes in extreme sea levels and coastal flood risk due to long-term tidal cycles. *Journal of Geophysical Research: Oceans*, *127*(4), e2021JC018157. https://doi.org/10.1029/2021JC018157

Falasca, F., Brettin, A., Zanna, L., Griffies, S. M., Yin, J., & Zhao, M. (2023). Exploring the nonstationarity of coastal sea level probability distributions. *Environmental Data Science*, *2*, e16. https://doi.org/10.1017/eds.2023.10

Feser, F., Barcikowska, M., Krueger, O., Schenk, F., Weisse, R., & Xia, L. (2015). Storminess over the North Atlantic and northwestern Europe—A review. *Quarterly Journal of the Royal Meteorological Society*, *141*(687), 350–382. https://doi.org/10.1002/qj.2364

Gan, B., & Wu, L. (2014). Centennial trends in northern hemisphere winter storm tracks over the twentieth century: Centennial trends in northern hemisphere winter storm tracks. *Quarterly Journal of the Royal Meteorological Society*, *140*(683), 1945–1957. https://doi.org/10.1002/qj.2263

Gill, A. E. (1982). *Atmosphere-ocean dynamics* (Nachdr. ed., Vol. 30). Academic Press.

Hague, B. S., Jones, D. A., Jakob, D., McGregor, S., & Reef, R. (2022). Australian coastal flooding trends and forcing factors. *Earth's Future*, *10*(2), e2021EF002483. https://doi.org/10.1029/2021EF002483

Haigh, I. D., Marcos, M., Talke, S. A., Woodworth, P. L., Hunter, J. R., Hague, B. S., et al. (2022). GESLA version 3: A major update to the global higher-frequency sea-level dataset. *Geoscience Data Journal*, *10*(3), 293–314. https://doi.org/10.1002/gdj3.174

Haigh, I. D., Nicholls, R., & Wells, N. (2010). Assessing changes in extreme sea levels: Application to the English Channel, 1900–2006. *Continental Shelf Research*, *30*(9), 1042–1055. https://doi.org/10.1016/j.csr.2010.02.002

Haigh, I. D., Pickering, M. D., Green, J. A. M., Arbic, B. K., Arns, A., Dangendorf, S., et al. (2020). The tides they are A-Changin': A comprehensive review of past and future nonastronomical changes in tides, their driving mechanisms, and future implications. *Reviews of Geophysics*, *58*(1), e2018RG000636. https://doi.org/10.1029/2018RG000636

Haigh, I. D., Wadey, M. P., Wahl, T., Ozsoy, O., Nicholls, R. J., Brown, J. M., et al. (2016). Spatial and temporal analysis of extreme sea level and storm surge events around the coastline of the UK. *Scientific Data*, *3*(1), 160107. https://doi.org/10.1038/sdata.2016.107

Hersbach, H., Bell, B., Berrisford, P., Hirahara, S., Horányi, A., Muñoz-Sabater, J., et al. (2020). The ERA5 global reanalysis. *Quarterly Journal of the Royal Meteorological Society*, *146*(730), 1999–2049. https://doi.org/10.1002/qj.3803

Hersbach, H., Bell, B., Berrisford, P., Hirahara, S., Horányi, A., Muñoz-Sabater, J., et al. (2023). Complete ERA5 from 1940: Fifth generation of ECMWF atmospheric reanalyses of the global climate [Dataset]. *Copernicus Climate Change Service (C3S) Climate Data Store (CDS)*. https://doi.org/10.24381/CDS.143582CF

Horsburgh, K. J., & Wilson, C. (2007). Tide-surge interaction and its role in the distribution of surge residuals in the North Sea. *Journal of Geophysical Research*, *112*(C8), C08003. https://doi.org/10.1029/2006JC004033

Hoskins, B. J., & Hodges, K. I. (2002). New perspectives on the northern hemisphere winter storm tracks. *Journal of the Atmospheric Sciences*, *59*(6), 1041–1061. https://doi.org/10.1175/1520-0469(2002)059⟨1041:NPOTNH⟩2.0.CO;2

Hoskins, B. J., & Hodges, K. I. (2019). The annual cycle of northern hemisphere storm tracks. Part II: Regional detail. *Journal of Climate*, *32*(6), 1761–1775. https://doi.org/10.1175/JCLI-D-17-0871.1

Idier, D., Bertin, X., Thompson, P., & Pickering, M. D. (2019). Interactions between Mean Sea Level, tide, surge, waves and flooding: Mechanisms and contributions to Sea Level variations at the coast. *Surveys in Geophysics*, *40*(6), 1603–1630. https://doi.org/10.1007/s10712-019-09549-5

Jenkins, L. J., Haigh, I. D., Camus, P., Pender, D., Sansom, J., Lamb, R., & Kassem, H. (2023). The temporal clustering of storm surge, wave height, and high sea level exceedances around the UK coastline. *Natural Hazards*, *115*(2), 1761–1797. https://doi.org/10.1007/s11069-022-05617-z

Knapp, K. R., Kruk, M. C., Levinson, D. H., Diamond, H. J., & Neumann, C. J. (2010). The international best track archive for climate stewardship (IBTrACS): Unifying tropical cyclone data. *Bulletin of the American Meteorological Society*, *91*(3), 363–376. https://doi.org/10.1175/2009BAMS2755.1

Lavaud, L., Pezerat, M., Coulombier, T., Bertin, X., & Martins, K. (2020). Hydrodynamics on a Rocky shore under moderate-energy wave conditions. *Journal of Coastal Research*, *95*(sp1), 1473. https://doi.org/10.2112/SI95-284.1

Liu, Z., Wang, H., Zhang, Y. J., Magnusson, L., Loftis, J. D., & Forrest, D. (2020). Cross-scale modeling of storm surge, tide, and inundation in mid-Atlantic bight and New York city during hurricane Sandy, 2012. *Estuarine, Coastal and Shelf Science*, *233*, 106544. https://doi.org/10.1016/j.ecss.2019.106544

MacMahan, J. (2015). Low-frequency seiche in a large bay. *Journal of Physical Oceanography*, *45*(3), 716–723. https://doi.org/10.1175/JPO-D-14-0169.1

MacPherson, L. R., Arns, A., Dangendorf, S., Vafeidis, A. T., & Jensen, J. (2019). A stochastic extreme Sea Level model for the German Baltic Sea coast. *Journal of Geophysical Research: Oceans*, *124*(3), 2054–2071. https://doi.org/10.1029/2018JC014718

Marciano, C. G., Lackmann, G. M., & Robinson, W. A. (2015). Changes in U.S. East coast cyclone dynamics with climate change. *Journal of Climate*, *28*(2), 468–484. https://doi.org/10.1175/JCLI-D-14-00418.1

Marcos, M., & Woodworth, P. L. (2017). Spatiotemporal changes in extreme sea levels along the coasts of the North Atlantic and the Gulf of Mexico. *Journal of Geophysical Research: Oceans*, *122*(9), 7031–7048. https://doi.org/10.1002/2017JC013065

Masselink, G., Scott, T., Poate, T., Russell, P., Davidson, M., & Conley, D. (2016). The extreme 2013/2014 winter storms: Hydrodynamic forcing and coastal response along the southwest coast of England. *Earth Surface Processes and Landforms*, *41*(3), 378–391. https://doi.org/10.1002/esp.3836

Mawdsley, R. J., & Haigh, I. D. (2016). Spatial and temporal variability and long-term trends in skew surges globally. *Frontiers in Marine Science*, *3*. https://doi.org/10.3389/fmars.2016.00029

Menéndez, M., & Woodworth, P. L. (2010). Changes in extreme high water levels based on a quasi-global tide-gauge data set. *Journal of Geophysical Research*, *115*(C10), 2009JC005997. https://doi.org/10.1029/2009JC005997

Munroe, R., & Curtis, S. (2017). Storm surge evolution and its relationship to climate oscillations at Duck, NC. *Theoretical and Applied Climatology*, *129*(1–2), 185–200. https://doi.org/10.1007/s00704-016-1770-5

Oppenheimer, M., Glavovic, B. C., Hinkel, J., van de Wal, R., Magnan, A. K., Abd-Elgawad, A., et al. (2019). Sea level rise and implications for low-lying islands, coasts and communities [Book Section]. In H.-O. Pörtner, D. C. Roberts, V. Masson-Delmotte, P. Zhai, M. Tignor, E. Poloczanska, et al. (Eds.), *IPCC special report on the ocean and cryosphere in a changing climate* (pp. 321–445). Cambridge University Press. https://doi.org/10.1017/9781009157964.006

Park, J., MacMahan, J., Sweet, W. V., & Kotun, K. (2016). Continuous seiche in bays and harbors. *Ocean Science*, *12*(2), 355–368. https://doi.org/10.5194/os-12-355-2016

Peng, M., Xie, L., & Pietrafesa, L. J. (2006). Tropical cyclone induced asymmetry of sea level surge and fall and its presentation in a storm surge model with parametric wind fields. *Ocean Modelling*, *14*(1–2), 81–101. https://doi.org/10.1016/j.ocemod.2006.03.004

Pineau-Guillou, L., Bouin, M.-N., Ardhuin, F., Lyard, F., Bidlot, J.-R., & Chapron, B. (2020). Impact of wave-dependent stress on storm surge simulations in the North Sea: Ocean model evaluation against in situ and satellite observations. *Ocean Modelling*, *154*, 101694. https://doi.org/10.1016/j.ocemod.2020.101694

Pineau-Guillou, L., Delouis, J., & Chapron, B. (2023). Characteristics of storm surge events along the North-East Atlantic coasts. *Journal of Geophysical Research: Oceans*, *128*(4), e2022JC019493. https://doi.org/10.1029/2022JC019493

Pineau-Guillou, L., Lazure, P., & Wöppelmann, G. (2021). Large-scale changes of the semidiurnal tide along North Atlantic coasts from 1846 to 2018. *Ocean Science*, *17*(1), 17–34. https://doi.org/10.5194/os-17-17-2021

Priestley, M. D. K., Dacre, H. F., Shaffrey, L. C., Schemm, S., & Pinto, J. G. (2020). The role of secondary cyclones and cyclone families for the North Atlantic storm track and clustering over western Europe. *Quarterly Journal of the Royal Meteorological Society*, *146*(728), 1184–1205. https://doi.org/10.1002/qj.3733

Priestley, M. D. K., Pinto, J. G., Dacre, H. F., & Shaffrey, L. C. (2017). The role of cyclone clustering during the stormy winter of 2013/2014. *Weather*, *72*(7), 187–192. https://doi.org/10.1002/wea.3025

Pugh, D., & Woodworth, P. (2014). *Sea-level science: Understanding tides, surges, tsunamis and mean sea-level changes* (1st ed.). Cambridge University Press. https://doi.org/10.1017/CBO9781139235778

Rabinovich, A. (2009). Seiches and harbor oscillations. In *Handbook of coastal and ocean engineering* (pp. 193–236). https://doi.org/10.1142/9789812819307_0009

Reinert, M., Pineau-Guillou, L., Raillard, N., & Chapron, B. (2021). Seasonal shift in storm surges at brest revealed by extreme value analysis. *Journal of Geophysical Research: Oceans*, *126*(12), e2021JC017794. https://doi.org/10.1029/2021JC017794

Schmitt, F. G., Crapoulet, A., Hequette, A., & Huang, Y. (2018). Nonlinear dynamics of the sea level time series in the eastern English Channel. *Natural Hazards*, *91*(1), 267–285. https://doi.org/10.1007/s11069-017-3125-7

Sebastian, A., Proft, J., Dietrich, J. C., Du, W., Bedient, P. B., & Dawson, C. N. (2014). Characterizing hurricane storm surge behavior in Galveston Bay using the SWAN+ADCIRC model. *Coastal Engineering*, *88*, 171–181. https://doi.org/10.1016/j.coastaleng.2014.03.002

Seneviratne, S., Zhang, X., Adnan, M., Badi, W., Dereczynski, C., Di Luca, A., et al. (2021). Weather and climate extreme events in a changing climate supplementary material [Book Section]. In V. Masson-Delmotte et al. (Eds.), *Climate change 2021: The physical science basis. contribution of working group i to the sixth assessment report of the intergovernmental panel on climate change (Chapter 11)*. University Press.

Stanev, E., Pein, J., Grashorn, S., Zhang, Y., & Schrum, C. (2018). Dynamics of the Baltic Sea straits via numerical simulation of exchange flows. *Ocean Modelling*, *131*, 40–58. https://doi.org/10.1016/j.ocemod.2018.08.009

Talke, S. A., Orton, P., & Jay, D. A. (2014). Increasing storm tides in New York Harbor, 1844-2013: INCREASING_stormtides_ny_1844to2013. *Geophysical Research Letters*, *41*(9), 3149–3155. https://doi.org/10.1002/2014GL059574

Thompson, P. R., Mitchum, G. T., Vonesch, C., & Li, J. (2013). Variability of winter storminess in the eastern United States during the twentieth century from tide gauges. *Journal of Climate*, *26*(23), 9713–9726. https://doi.org/10.1175/JCLI-D-12-00561.1

Wahl, T., & Chambers, D. P. (2015). Evidence for multidecadal variability in US extreme sea level records. *Journal of Geophysical Research: Oceans*, *120*(3), 1527–1544. https://doi.org/10.1002/2014JC010443

Wahl, T., & Chambers, D. P. (2016). Climate controls multidecadal variability in U. S. extreme sea level records. *Journal of Geophysical Research: Oceans*, *121*(2), 1274–1290. https://doi.org/10.1002/2015JC011057

Wahl, T., Mudersbach, C., & Jensen, J. (2011). Assessing the hydrodynamic boundary conditions for risk analyses in coastal areas: A stochastic storm surge model. *Natural Hazards and Earth System Sciences*, *11*(11), 2925–2939. https://doi.org/10.5194/nhess-11-2925-2011

Wolf, J., & Flather, R. (2005). Modelling waves and surges during the 1953 storm. *Philosophical Transactions of the Royal Society A: Mathematical, Physical & Engineering Sciences*, *363*(1831), 1359–1375. https://doi.org/10.1098/rsta.2005.1572

Woodworth, P. L., Hunter, J. R., Marcos, M., Caldwell, P., Menéndez, M., & Haigh, I. (2016). Towards a global higher-frequency sea level dataset. *Geoscience Data Journal*, *3*(2), 50–59. https://doi.org/10.1002/gdj3.42

Zhang, K., Douglas, B. C., & Leatherman, S. P. (2000). Twentieth-century storm activity along the U.S. East coast. *Journal of Climate*, *13*(10), 1748–1761. https://doi.org/10.1175/1520-0442(2000)013⟨1748:TCSAAT⟩2.0.CO;2